Repulsive forces between neutral surfaces induced by adatoms

Han Hu,[1] Kun Ding,[2] T. C. Leung,[1,*] and C. T. Chan[2,†]

[1]*Department of Physics, National Chung Cheng University, Chia-Yi 62101, Taiwan*
[2]*Department of Physics and Institute for Advanced Study, The Hong Kong University of Science and Technology, Clear Water Bay, Hong Kong*

Charge neutral objects usually attract each other in the nanoscale and it is actually not favorable for nanoscale manipulation as attractive forces tend to make objects stick together. It would be highly desirable if the sign of the force between charge neutral objects could be controlled by surface chemical modification. In this work, we show that the static electric field generated by a submonolayer of chemisorbed adatoms can be used to control the sign of the forces between neutral surfaces. The local density functional method combined with an electrostatic stress tensor approach is used to study the forces between tungsten surfaces with stripes of noble metal atoms adsorbed on top. When the metal substrate is partially covered by the adatom stripes, the electric field generated by the local variation of the work function can extend into the vacuum, which in turn can attract or repel other surfaces in close vicinity. Chemisorption may hence offer a good strategy to manipulate nanoscale objects.

I. INTRODUCTION

When two objects are so close to each other that their valence electrons start to overlap, their mutual interaction will be dominated by forces due to chemical bonding. When they are further separated, charge neutral objects can still attract each other through quantum fluctuation forces such as van der Waals and Casimir forces [1–3]. The fact that van der Waals forces are always attractive may not be optimal for nanotechnology, as the attraction may make nanomanipulators or molecular assemblers tend to stick to the nano-objects that they want to manipulate. It is highly desirable to have surface modification strategies that can modify the forces between neutral objects so that they are not always attractive. While Casimir forces are generally attractive, it has been demonstrated recently that the Casimir forces between two surfaces can be made repulsive in some special configurations, such as by introducing liquids [4,5], creating artificial materials with unusual effective material dispersions [6–11], or via corrugation [12,13]. More examples of nonattractive dispersive forces due to materials at the nanoscale or nontrivial boundary conditions can be found in comprehensive reviews [14,15]. It has also been shown that the forces between neutral corrugated plasmonic surfaces can be either attractive or repulsive [16], and this type of corrugation-induced force is a geometric effect related to the ground-state electron distribution, and has nothing to the fluctuation effects that lead to Casimir or van der Waals forces.

In this work, we show that change of local work function induced by a monolayer of adsorbates can also be used to control the sign of the forces between two surfaces. We will use the local density functional method [17–21] to study the forces between tungsten surfaces with stripes of noble metal atoms adsorbed on top. The adsorbate atoms modify the local work function of the substrate and when the metal substrate is not completely covered, the electric field generated by the local variation of work function can extend into the vacuum, which in turn induces forces on surfaces in close vicinity. The force can be attractive or repulsive and the fact that its sign can be controlled offers a good strategy to manipulate nanoscale objects. The paper is organized as follows. In Sec. II, we show the forces between surfaces can be attractive or repulsive, which depends on the details of the adsorbate covering the substrate. In Sec. III, we demonstrate the robustness of such repulsive force, including the geometric dependence, the relaxation effect, and different types of adatoms. Conclusions are drawn in Sec. IV.

II. REPULSIVE FORCES INDUCED BY ADSORBATE

We will use tungsten (W) as our prototypical substrate and gold (Au) as the absorbate. Let us start from W(001) surfaces with stripes of atoms adsorbed on top, as shown in Figs. 1(a)–1(d), where the black open circles represent W atoms and the red solid circles represent absorbate atoms. A seven-layer slab in supercell configuration is used to model the W(001) surface. The surface is partially covered by stripes of Au atoms adsorbed on the hollow sites, forming locally a (1×1) Au/W(001) configuration. Previous results show that the chemisorption can induce significant changes in the work function, with the sign and magnitude depending on the adatom [22]. The Au adsorbates aggregate into stripes, and in the configuration shown in Fig. 1, the stripes cover half of the W(001) surface area. We use the symbols N_W and N_{Au} to denote, respectively, the number of W atoms in the uppermost W layer and the number of Au adatoms in the supercell. The Au stripes on the top and the bottom surfaces are arranged so that their registry with the W substrate can be shifted by an amount denoted by N_{shift}, which is the number of W lattice constants that the Au stripes on the top are shifted

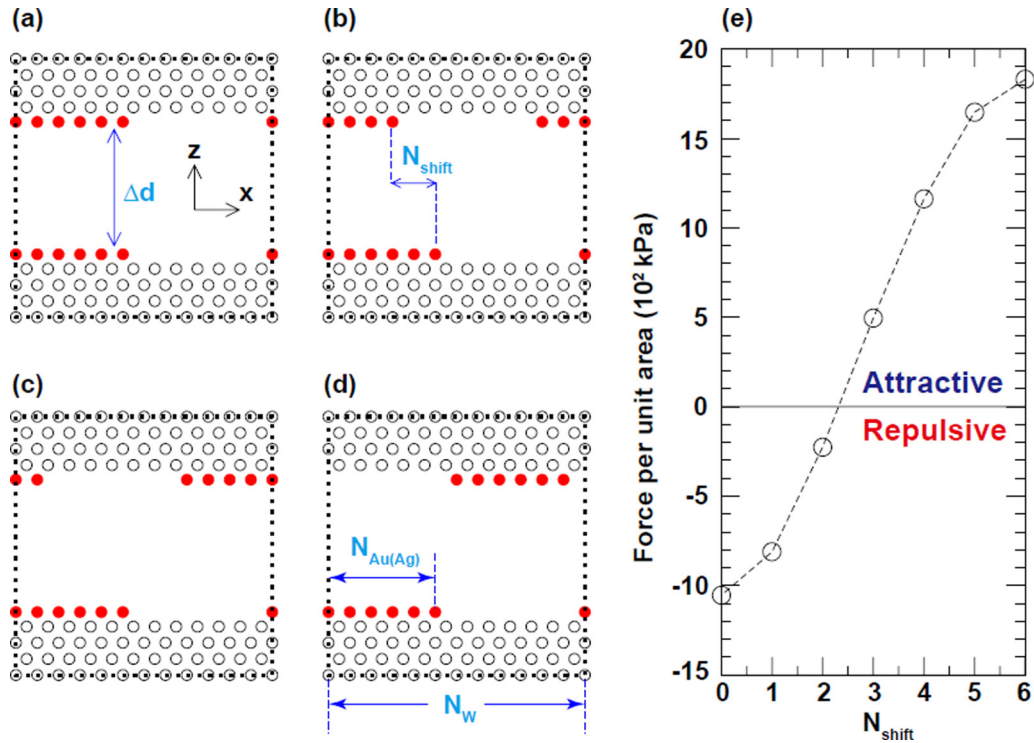*tcleungtw@gmail.com
†phchan@ust.hk

FIG. 1. Schematic picture of Au/W slab structure. The solid red circles denote Au atoms and black open circles represent W atoms. The black dashed lines mark the primitive supercell boundaries in the calculation. The distance between these slabs is Δd. The numbers of surface W atoms and Au adatoms along the x direction are represented by $N_W = 12$ and $N_{Au} = 6$, respectively. The $N_{shift} = 0, 2, 4,$ and 6 cases are shown in panels (a–d), respectively. (e) The electrostatic forces per unit area calculated by the surface integral of the electrostatic stress tensor for Au/W slab structure with $N_W = 12$, $N_{Au} = 6$, and $\Delta d = 13$ Å as a function of N_{shift} are shown by open black circles. The negative (positive) number means repulsive (attractive) forces between these slabs. The dotted line is a guide to the eye.

relative to the stripes at the bottom surface. Figures 1 and 2 consider the situation when $N_W = 12$ and $N_{Au} = 6$. When $N_{shift} = 0$, the Au stripes on the bottom surface are the mirror images of those on the top with respect to the mirror plane at the middle of the W slab. In the repeated-slab configuration, as shown in Fig. 1(a), the Au adatoms on top of one slab will see the Au atoms on the bottom of an adjacent slab directly above it, separated by the vacuum in the supercell. When $N_{shift} = 6$, the lateral shift is half a unit cell along the x direction [see Fig. 1(d)]. In this case, the Au adatoms on the top of one slab will face bare W substrate across the vacuum in the repeated-slab configuration. For intermediate values of N_{shift}, the Au atoms on top of one slab will face partly Au atoms and partly uncovered W surface atoms on the bottom of the slab above it across the vacuum.

We then calculate the forces between the slabs. For simplicity, we keep the W atoms in their ideal positions. The experimental lattice constant of W ($a = 3.19$ Å) is used in the calculation. We put the Au atoms in the hollow site, which is the most favorable site for Au adsorption. The Au-W distance was determined by a (1×1) surface unit cell calculation. We will show (qualitatively similar) results corresponding to fully relaxed atomic coordinates later, but it is much easier to explain the physics by keeping the W and Au top layer "flat" for the moment. We use standard local density functional procedures to find the electron density that minimizes the total energy. In the present calculations, the frozen-core full-potential projector augmented-wave (PAW)

method was used [17], as implemented in the Vienna *ab initio* simulation package (VASP) [18–20]. We adopted the Perdew-Burke-Ernzerhof generalized gradient approximation [21] for the exchange and correlation energy. The k-point grid is chosen with spacings that are smaller than $0.023 \, (2\pi/\text{Å})$. The ground-state electron density gives the corresponding electrostatic potential which is shown in Fig. 2 for the vacuum region of interest for various values of N_{shift}. The zero of the electrostatic potential is chosen to be the mean value of the electrostatic potential inside the plot region. The gradient of the electrostatic potential in the vacuum region gives the electric field components, as shown by the vector fields in the right panel of Fig. 2. Using the electric fields in the vacuum region, the electrostatic forces can be calculated by doing the surface integral of the electrostatic stress tensor $\mathbf{T}$ at the middle of the vacuum where the electronic charge is zero:

$$\mathbf{F}_\alpha = \int \sum_{\beta = x, y, z} \mathbf{T}_{\alpha\beta} n_\beta \, dS, \tag{1}$$

where α, β denotes the components of certain vectors and tensors, $\mathbf{n}$ is the outward normal to the surface, dS is the infinitesimal area of the surface, the electrostatic stress tensor is

$$\mathbf{T}_{\alpha\beta} = \varepsilon_0 \left[\mathbf{E}_\alpha \mathbf{E}_\beta - \frac{1}{2} (\mathbf{E} \cdot \mathbf{E}) \delta_{\alpha\beta} \right], \tag{2}$$

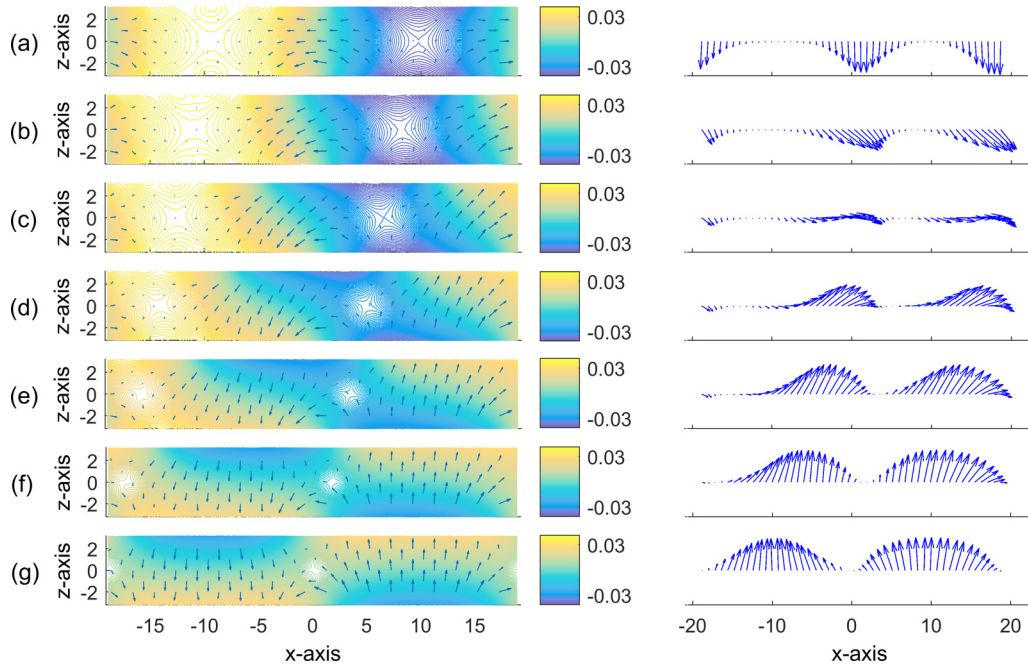FIG. 2. The left panels show the electrostatic potential in units of eV (color map) and the corresponding electric field (vector field) for $N_{shift} = 0, 1, 2, 3, 4, 5$, and 6 are shown in the left panel of (a–g), respectively. The zero of the z axis is chosen to be at the middle of the vacuum. The units in the x axis and z axis are in angstroms. The right panels show the direction and the relative magnitude of the electrostatic force density calculated at the center of the vacuum gap ($z = 0$). The system parameters are $N_W = 12$, $N_{Au} = 6$, and $\Delta d = 13$ Å. If the force density vector points up (down), the force between the slabs is attractive (repulsive). Panel (a) shows that for the symmetric $N_{shift} = 0$ configuration, the repulsive force is mainly localized at the edge of the Au stripe. Panel (g) shows that for the asymmetric $N_{shift} = 6$ configuration, the attractive force is strongest in the middle of the stripe.

and **E** is the electrostatic fields generated by all the charges. As long as the vacuum is thick enough, the electronic density at the middle of the vacuum is essentially zero. In that case, the force calculated using the electrostatic tensor is by definition an electrostatic force, with no chemical (bonding) or quantum fluctuation (such as van der Waals or Casimir) effects. In this case, the vacuum thickness of 13 Å is already thick enough to ensure that the ground-state electron density is negligibly small at the integration surface. We purposely change the electrostatic tensor integration surface 1 Å above and below the middle of the vacuum, and the forces are found to be same. More details about the electrostatic stress tensor approach are given in Appendix A, where we show that doing a boundary integral for the electrostatic stress tensor to get the total force is equivalent to doing a volume integration of charge and field. In principle, the electrostatic forces can also be extracted directly using a finite difference of the total energies as the vacuum thickness is varied. As shown in Appendix B, we show that the electrostatic stress tensor approach is a more elegant and numerically stable approach to obtain the electrostatic force due to the field in vacuum.

Figure 1(e) shows the electrostatic forces per unit area that act between the slabs. A positive (negative) number indicates attraction (repulsion). When we arrange the patterned W surfaces so that the Au stripes on one surface directly face the Au stripes of the other surface ($N_{shift} = 0$), the two surfaces repel each other. When the Au stripes of the surface are in a staggered formation ($N_{shift} = 6$), the force becomes attractive. It is quite natural that there must be some intermediate value of N_{shift} such that the forces becomes zero. The sign of the

forces can be explained when we look at the field distribution, which is shown in Fig. 2 for various values of N_{shift}. We see that when $N_{shift} = 6$, the field lines point from the Au adatoms of one surface to the bare W surface atoms of the other surface, as shown by vector fields in the left panel of Fig. 2(g). The "vertical" field lines that connect the two surfaces cause attraction between them. When $N_{shift} = 0$, the field lines point from the adatoms of one surface to the bare W surface on the same surface, as shown by vector fields in the left panel of Fig. 2(a). The "lateral" field lines induce repulsion between surfaces.

To further understand the sign of the forces, we show the force distributions in the right panels of Fig. 2, where we plot the force density defined by

$$f_\alpha = \sum_{\beta=x,y,z} T_{\alpha\beta} n_\beta a_y. \tag{3}$$

Here, a_y is the length of the unit cell along the y direction. The total force between the slabs is the line integrals of the force density along the x direction. We use the sign convention that if $f_z > 0 (f_z < 0)$, it is an attraction (repulsion) between the surfaces. So, if the arrows point up ($f_z > 0$) in the right panels, the two surfaces are attracting each other. We note that only the total force, as defined in Eq. (1), is an experimentally measured quantity but the force density can offer us an intuitive understanding of the force distribution. Let us first examine the staggered configuration ($N_{shift} = 6$), shown in the lowest panels [Fig. 2(g)]. The left panel shows that field lines pointing up/down connecting the Au and W atoms on

two surfaces causing an attraction are strongest in the interior of the stripe. However, the fields near the edge of the strip are not pointing up/down, but are bending over to connect the edge Au atoms with the exposed substrate W atoms near the edge. These field lines do not contribute to attraction. This is consistent with the force density shown on the right panel of Fig. 2(g). We see that the attractive force density is essentially zero near the edge, but reaches a maximum near the middle of the stripe. For the symmetric configuration ($N_{shift} = 0$), the force density pattern is strong only at boundary of the strip [the right panel in Fig. 2(a)], and it is a repulsive force as the arrows are pointing down. This is consistent with the electric field pattern shown in the left panel. For intermediate values of N_{shift}, the force density vectors have more complex twisting patterns [right panels from Fig. 2(b) to 2(f)], and they sum up to a very small number.

It is quite clear from the results shown in Fig. 2 that the attractive/repulsive forces originate from the electric field coming out of the partially exposed W surface. As the electron affinity of the adsorbed atom is different from that of the substrate atoms, some charge transfer between adsorbate/substrate will be inevitable. If the adsorbates completely cover the substrate, the adsorption induces a uniform change of the work function across the surface, for instance, an increase of 0.7 eV in a (1×1) unit cell if we use Au as adsorbate [22]. In that case, the electric field in the vacuum a few angstroms from the surface will be essentially zero and there is no electrostatic force that can be induced between surfaces. If the adsorbate forms patches or stripes so that the coverage is incomplete, there must be some electric field in the vacuum close to the surface. From a macroscopic viewpoint, the coverage of adsorbed species changes the work function locally and a local variation of work function causes electric fields spilling into the vacuum region.

III. ROBUSTNESS OF REPULSIVE FORCES

We have already shown that the sign of electrostatic forces can be controlled by relative positions of adatoms, which is a useful way to achieve repulsion between nanoscale neutral surfaces. Other forces at work in the nanoscale, such as van der Waals and Casimir forces, tend to be attractive in nature, and hence achieving repulsion using local variation of work function is more interesting and more useful than achieving attraction. In view of this reason, we focus on the robustness of the repulsive force in the following section.

As the surface covered with stripes of adsorbates is overall neutral, the patch fields must decay into the vacuum and hence the electrostatic force due to those fields should be a short-ranged force. In Fig. 3, we examine the range of this force by considering the force as a function of the vacuum thickness Δd. The coverage of the stripes is kept at half, i.e., $N_W = 2N_{Au}$. We show results of the symmetric ($N_{shift} = 0$) configuration which gives the strongest repulsion for a few unit cell sizes, corresponding to different widths of the Au stripes. In Fig. 3(a), the W atomic distances are kept at ideal bulk values, and in Fig. 3(b) the atomic coordinates are fully relaxed. The numerical results can be summarized as follows. Firstly, independent of the width of the Au stripe, the symmetric configuration ($N_{shift} = 0$) gives rise to repulsion, and the

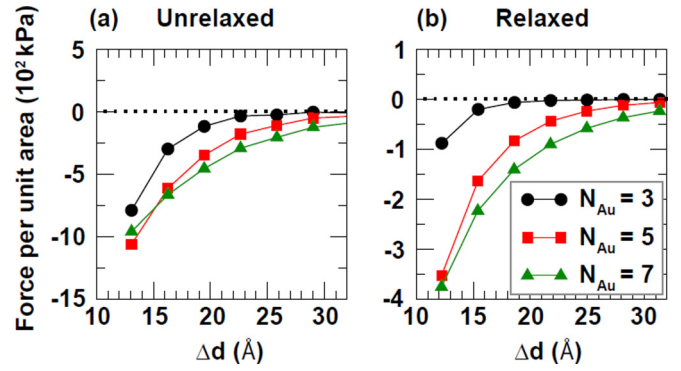FIG. 3. The electrostatic repulsive forces per unit area for the $N_{Au} = 3$, $N_{Au} = 5$, and $N_{Au} = 7$ slab structures as a function of Δd are shown by black, red, and green lines, respectively, for $N_{shift} = 0$. We fix $N_W = 2N_{Au}$ (i.e., half the W surface is covered by Au). The atomic structure in (a) is chosen at the ideal position and the atomic structures are fully relaxed in (b). The line between the points is a guide to the eye.

force per unit cell is generally stronger when the adsorbate stripe is wider. The magnitude of the force drops off quite quickly as a function of distance, in agreement with the fact that the electric field must decay for an overall neutral surface. If we take the sea-level atmospheric pressure ($\sim$100 kPa) as a reference, the force per unit area is appreciable at distances smaller than 20 Å. In Fig. 3(b), we show results corresponding to fully relaxed atomic coordinates. The overall results are qualitatively similar to that shown in Fig. 3(a) for unrelaxed coordinates. After relaxation, the Au adatoms remain in the hollow sites but there is some buckling of the top layer. We found that the variation of Au-W atomic distances within the stripe tend to reduce the field strength in the vacuum, with the consequences that the attractive/repulsive force becomes smaller.

We next examine in greater detail the dependence of the force on the width of the stripe. In Fig. 4(a), the filled and open black circles represent results for Au/W of unrelaxed and relaxed atomic coordinates, respectively. We maintain
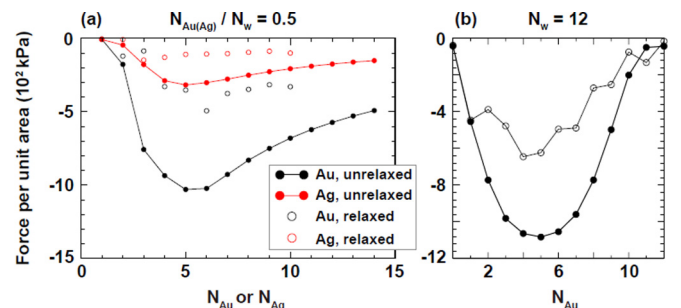

FIG. 4. (a) The electrostatic repulsive forces per unit area for Au/W and Ag/W slab structures as a function of $N_{Au(Ag)}$ for the fixed ratio $N_W = 2N_{Au(Ag)}$ are shown by black and red dots, respectively. (b) The electrostatic forces for the Au/W slab structure for $N_w = 12$ as a function of N_{Au} are shown by black dots. The filled and open circles in both figures denote unrelaxed and relaxed results, respectively. The used parameters are $\Delta d = 13$ Å and $N_{shift} = 0$. The line between the points is a guide to the eye.
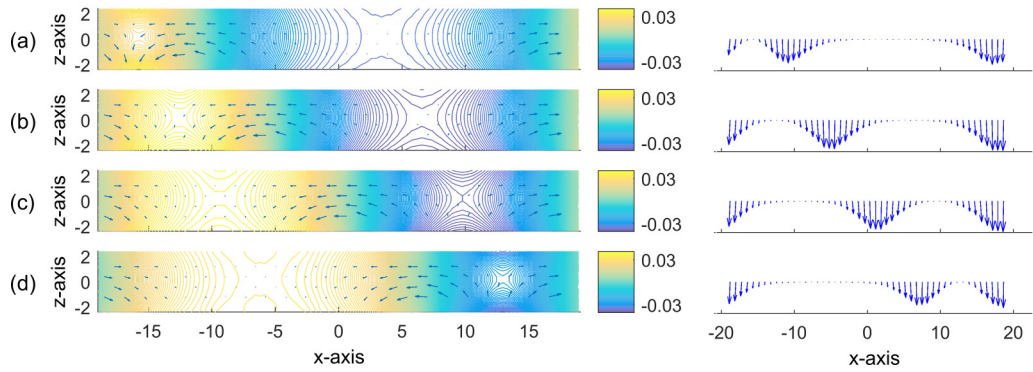
FIG. 5. Plot of the electrostatic potential in units of eV (color map) and the corresponding electric field (vector field) for $N_{Au} = 2, 4, 6$, and 8 are shown in the left panel of (a–d), respectively. The zero of the z axis is chosen to be at the middle of the vacuum. The units in the x axis and z axis are in angstroms. The right panels show the direction and the relative magnitude of the electrostatic force density calculated at the center of the vacuum region. The system parameters are $N_W = 12$, $N_{shift} = 0$, and $\Delta d = 13$ Å.

half coverage so that $N_W = 2N_{Au}$. In this case, the force is repulsive, but the force per unit cell does not change monotonically. It reaches a maximum and then decreases as the stripe grows wider. We can understand the trend by examining the electric field and force field patterns, shown in Fig. 2(a). In the symmetric configuration ($N_{shift} = 0$), reflection symmetry dictates that the electric field at the middle of the vacuum should be zero for a (1×1) configuration. So, if the stripe is wide enough, surface atoms near the center of the stripe cannot contribute to the force between different surfaces. Only the edge can contribute. This shows up quite clearly in the right panel of Fig. 2(a), which indicates that the force density is appreciable only near the edge as discussed previously. When the stripe is too narrow, the edge is not that well defined, so the force is weak. When the stripe grows wider and wider, the ratio of the number of edge atoms to the interior atoms decreases, and the force per unit area should decrease. The force hence reaches a maximum at some values of the stripe width in which the edge becomes well defined while the number of edge atoms is not small compared with the number of Au adatoms in the interior of the stripe. The results corresponding to fully relaxed atomic coordinates show that the repulsive force becomes smaller if the surface layers are allowed to buckle, which tends to reduce the field in the vacuum region. The repulsive force per unit area also reaches a maximum for some intermediate value of the stripe width, qualitatively similar to the results obtained with unrelaxed atomic positions.

In Fig. 4(a), we also present the corresponding results with Ag replacing Au as the adsorbate. The red solid and open circles represent, respectively, the forces calculated using unrelaxed and fully relaxed atomic coordinates. The results are very similar except that the forces are smaller. This can be explained by the fact that a monolayer of Ag induces a much smaller change of work function on the W substrate [an increase of only 0.05 eV in a (1×1) unit cell if we use Ag as adsorbate] [22]. This highlights the fact that the physics behind the observed effect is rather generic, and a larger adsorbate-induced change in local work function will induce a stronger effect.

We now consider the effect of the adsorbate coverage. In Fig. 4(b), we show results for repulsive forces between surfaces in the symmetric configuration ($N_{shift} = 0$) for various widths of the Au stripes, with the number of surface W atoms fixed at $N_W = 12$. The width of the stripe, and hence the coverage, depends on the number of Au atoms adsorbed. The $N_{Au} = 0$ configuration corresponds to a clean W surface and $N_{Au} = 12$ means complete coverage by Au [i.e., (1×1) Au/W(100) surface]. For these two extreme cases, the force should be zero, and indeed the forces are found numerically to be essentially zero. The force must reach a maximum at some intermediate values of the stripe width and indeed the repulsive force is found to be strongest when the stripe covers approximately half of the surface. This is also because the repulsive force mainly occurs at the edge between Au covered surfaces and clean surfaces. Unrelaxed (solid circles) and fully relaxed (open circles) atomic coordinates give qualitatively similar results. The surface relaxation tends to reduce the repulsion but the qualitative behavior is similar. The line joining the open circles corresponding to relaxed coordinates is not as smooth as that joining the solid circles as the surface displacements for intermediate values of coverage are rather complex.

Figure 5 shows the potential and field distribution (left panels) and the force density distribution (right panels) for $N_{Au} = 2, 4, 6$, and 8 for the configurations corresponding to data points shown as solid black dots in the Fig. 4(a). We see that the force density is strongest near the edge and the force field tends to be stronger when the edges are far away from each other.

IV. DISCUSSION AND CONCLUSION

In this work, we are calculating ground-state forces (fluctuating forces are consequences of second-order perturbation, and not a ground-state effect). It would be interesting to compare the electrostatic force with van der Waals or Casimir forces for these systems, but these would be challenging calculations. We note that we cannot just use the Lifshitz-type formula for Casimir forces to calculate the fluctuation force for the systems we are working with. The Lifshiftz formula assumes that the material is described by a dielectric function and a typical Casimir force calculation will take the bulk dielectric function documented in handbooks. These nanoscale

surface systems with submonolayer chemical adatoms cannot be described by a simple dielectric function, and we need to consider complications arising from nonlocal effects due to corrugation and electron spill-out effect that cannot be ignored in the nanoscale. The Lifshitz-type formula also requires a geometric boundary, which is not well defined here because the adatom stripes induce surface corrugation and there is no well-defined way to draw a geometric boundary between materials [atoms in local density approximation (LDA) calculations] and vacuum (which contains an electronic charge close to the surface). A fair comparison would be a van der Waals force calculation at the DFT level, which will be very computationally challenging.

In short, we have presented a unique kind of force working at the nanoscale between surfaces partially covered by adatoms. Such forces originate from the modulation of local work functions caused by the adsorbate, leading to electric fields leaking into the vacuum. The force is strong if the adatoms can induce a large change in work function. The forces are obtained numerically using an electrostatic stress tensor with the electric fields determined using the local density functional approach. An interesting aspect is that the force between patterned surfaces can be repulsive in the range of 10–20 Å. Such forces may offer a good strategy to manipulate nanoscale objects if the surface can be modified by chemisorption.

ACKNOWLEDGMENTS

APPENDIX A: USING ELECTROSTATIC STRESS TENSOR TO CALCULATE FORCES

The Lagrangian for charges in the electrostatic field is

$$L = T - U = -\rho\phi, \tag{A1}$$

where ρ is the charge distribution, and ϕ is the Coulombic potential generated by all the charges (see, for example, the color map in the left panel of Figs. 2 and 5). By using the Euler-Lagrangian equation, we get the electrostatic force density at point r_i as

$$f_i = \frac{\partial L}{\partial r_i} = -\rho\partial_i\phi = \rho\mathbf{E}_i, \tag{A2}$$

where i stands for the ith component of the vector. The total electrostatic force of a particular object can be obtained by integrating the force density,

$$\mathbf{F} = \int_\Omega d\mathbf{r}\rho\mathbf{E}, \tag{A3}$$

where Ω stands for the domain of the object under consideration. In principle, the total electrostatic force of the Au-W slab in the main text can be obtained by performing the volume integral (A3) with the charge distribution obtained

using VASP or other methods that can determine the LDA charge density, but such a procedure may be tedious and numerically demanding because of the large charge density background near the atoms. A more elegant way to handle such a problem is to transform Eq. (A3) into a boundary integral equation as

$$
\begin{aligned}
\mathbf{F} &= \int_\Omega d\mathbf{r}\rho\mathbf{E} = \varepsilon_0 \int_\Omega d\mathbf{r}(\nabla\cdot\mathbf{E})\mathbf{E} \\
&= \varepsilon_0 \int_\Omega d\mathbf{r}[\nabla\cdot(\mathbf{E}\mathbf{E}) - (\mathbf{E}\cdot\nabla)\mathbf{E}] \\
&= \varepsilon_0 \int_\Omega d\mathbf{r}\left[\nabla\cdot(\mathbf{E}\mathbf{E}) - \frac{1}{2}\nabla(\mathbf{E}\cdot\mathbf{E})\right] \\
&= \varepsilon_0 \int_\Omega d\mathbf{r}\nabla\cdot\left[\mathbf{E}\mathbf{E} - \frac{1}{2}(\mathbf{E}\cdot\mathbf{E})\overleftrightarrow{\mathbf{I}}\right] \\
&= \int_{\partial\Omega} \mathbf{T}\cdot\mathbf{n}\,dS.
\end{aligned}
\tag{A4}
$$

The last step uses Gauss's law with the definition of an electrostatic stress tensor as

$$\mathbf{T} = \varepsilon_0\left[\mathbf{E}\mathbf{E} - \frac{1}{2}(\mathbf{E}\cdot\mathbf{E})\overleftrightarrow{\mathbf{I}}\right]. \tag{A5}$$

During the derivations in Eq. (A4), the following identities have been used:

$$\nabla\cdot(\mathbf{E}\mathbf{E}) = (\nabla\cdot\mathbf{E})\mathbf{E} + (\mathbf{E}\cdot\nabla)\mathbf{E}, \tag{A6}$$

$$\nabla(\mathbf{E}\cdot\mathbf{E}) = 2(\mathbf{E}\cdot\nabla)\mathbf{E} + 2\mathbf{E}\times(\nabla\times\mathbf{E}), \tag{A7}$$

$$\nabla\cdot(g\overleftrightarrow{\mathbf{I}}) = (\nabla g)\cdot\overleftrightarrow{\mathbf{I}} = \nabla g. \tag{A8}$$

Equation (A4) is the stress tensor method used in the main text. The second term on the right-hand side of Eq. (A7) is zero because we focus on electrostatics here. Comparing with Eq. (A7), the major advantage of the stress tensor method is that we only need to calculate the electrostatic field (the gradient of Coulombic potential) in the boundary enclosing the whole slab. We only need to do a boundary integral instead of a volume integral. The stress tensor method used in the main text offers a good numerical tool to study the electrostatic force between different objects.

APPENDIX B: FORCES CALCULATED BY THE GRADIENT OF ENERGY

The electrostatic force can also be calculated using the total energy obtained from VASP. Here, we compare the force between the slabs calculated using the gradient of the energy from the local density function calculation and that calculated using the electrostatic stress tensor approach. As an example, we consider the case of $N_{Au} = 5$ with $N_W = 2N_{Au}$. We use 3.2 Å as the lattice constant of W, and keep the W and Au atoms in their ideal positions. From a LDA point of view, we are actually calculating the electric field energy trapped in the vacuum region, which is a very small part of the total energy in the gigantic unit cell. Worse still, we need to compare the energy of supercells with different sizes as the distance of the
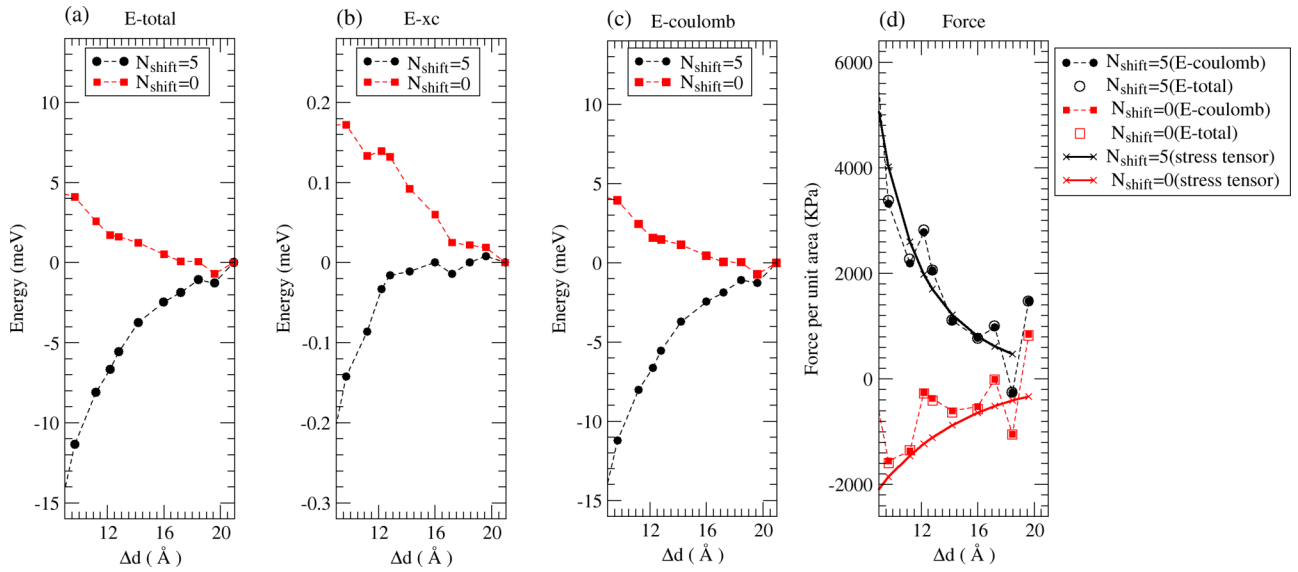
FIG. 6. The relative total energy (using $\Delta d = 20\,\text{Å}$ as a reference), relative exchange-correlation energy, relative Coulomb energy, the force calculated by the gradient of the Coulomb energy, and the force calculated by the surface integral of the electrostatic stress tensor as a function of interslab distance for $N_{\text{shift}} = 5$ and $N_{\text{shift}} = 0$. The system parameters are $N_{\text{Au}} = 5$ and $N_{\text{W}} = 2N_{\text{Au}}$.

slab needs to be changed in order to find the gradient of the energy as a function of the interslab interface. The calculated total energy is numerically sensitive to the number of grid points in the fast Fourier transform (FFT) mesh along the directions of the lattice vectors. The grid points along the z direction have to have been chosen very carefully to prevent the numerical noise due to the change of position of the grid in the slab when we increase the distance between the slabs (vacuum thickness of the unit cell). We take the number of grid points along the z direction as two per $0.1\,\text{Å}$. The FFT mesh (NGX, NGY, and NGZ in VASP) are factors of 2, 3, and 5 and hence only a few values of interslab distances are allowed. The grid points in the x-y plane were taken to be 320×32 and the k-point sampling was taken to be $4 \times 16 \times 4$. The relative total energy, relative exchange-correlation energy, relative Coulomb energy, and the force calculated by the gradient of the $N_{\text{Au}} = 5$ with $N_{\text{W}} = 2N_{\text{Au}}$ are shown in Fig. 6. We set the energies to be zero at $\Delta d = 20\,\text{Å}$ and use this as the reference. The choice of reference energy will not affect the calculation of the forces, which is the gradient of energy. For the case of $N_{\text{shift}} = 5$, with results marked by black dots in Fig. 6(a), the total energy increases as the interslab distance increases, which implies an attractive force between the slabs. For $N_{\text{shift}} = 0$, with results marked by red squares, the total energy decreases as the interslab distance increases, indicating a repulsive force between the slabs. This is consistent with the results obtained using the electrostatic stress tensor approach shown in the main text. The exchange-correlation energy for various values of interslab distance is shown in Fig. 6(b). We note that the magnitude of the relative exchange-correlation energy [Fig. 6(b)] is about 40 times smaller than that of relative total energy. That is because the charge density in the vacuum is very small. In Fig. 6(c), we subtract the small exchange-correlation energy contribution from the total energy difference to obtain the Coulomb energy due to the electric field in the vacuum region. We note that Fig. 6(c) is practically the same as Fig. 6(a). This means that

the change of energy as a function of interslab distance is essentially due to the electrostatic energy stored in vacuum. Taking a finite difference of the Coulomb energy shown in Fig. 6(c), we obtain the electrostatic force and results are shown as red and black solid symbols in Fig. 6(d) for $N_{\text{shift}} = 5$ and $N_{\text{shift}} = 0$, respectively. For completeness, we also show the force calculated by taking the finite difference of the total energy, as shown by the open symbols in Fig. 6(d), which are essentially the same as the solid symbols. For comparison, the forces calculated using the surface integral of the electrostatic stress tensor are also shown in Fig. 6(d) as solid black and
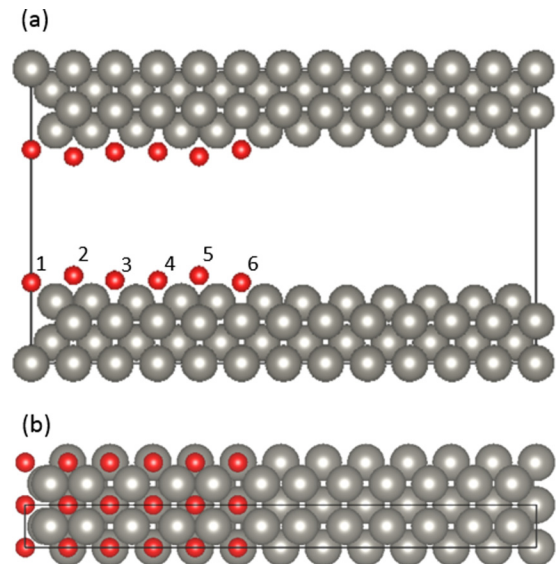

FIG. 7. Picture of (a) side view and (b) top view of relaxed Au/W slab structure with $N_{\text{W}} = 12$, $N_{\text{Au}} = 6$, $N_{\text{shift}} = 0$, and $\Delta d = 9\,\text{Å}$. The solid red circles denote Au atoms and black solid gray circles represent W atoms. The black lines mark the primitive supercell boundaries in the calculation.

TABLE I. The interatomic distance d (units of angstroms) of the nearest-neighbor atoms of the relaxed Au/W slab structure with $N_W = 12$, $N_{Au} = 6$, $N_{shift} = 0$, and $\Delta d = 9$ Å. $d(Au - Au)$ is the distance between two Au atoms and $d(Au - W)$ is the distance between the Au atom and the W atom.

Atom	$d(Au - Au)$	$d(Au - W)$
Au_1	$(3.190 \times 2, 3.239)$	$(2.806 \times 2, 2.848 \times 2)$
Au_2	$(3.155, 3.190 \times 2, 3.239)$	$(2.878 \times 2, 2.879 \times 2)$
Au_3	$(3.155, 3.190 \times 2, 3.260)$	$(2.830 \times 2, 2.871 \times 2)$
Au_4	$(3.155, 3.190 \times 2, 3.260)$	$(2.830 \times 2, 2.871 \times 2)$
Au_5	$(3.155, 3.190 \times 2, 3.239)$	$(2.878 \times 2, 2.879 \times 2)$
Au_6	$(3.190 \times 2, 3.239)$	$(2.806 \times 2, 2.848 \times 2)$

red lines and the results are in agreement with the results calculated by the gradient of LDA calculated energy. The forces calculated by the electrostatic stress tensor approach are smooth and are almost independent of the choice of k points and FFT mesh. On the other hand, the force calculated by the gradient of the total energy is numerically noisy and very sensitive to the sampling of k points and FFT mesh. The electrostatic stress tensor approach provides a practical and efficient way to evaluate the electrostatic force due to the electric field trapped in the vacuum region between the slabs.

APPENDIX C: ATOMIC STRUCTURE OF THE RELAXED Au/W SLAB STRUCTURE

The relaxed Au/W slab structure with $N_W = 12$, $N_{Au} = 6$, $N_{shift} = 0$, and $\Delta d = 9$ Å is shown in Fig. 7. Since we use a seven-layer slab in the supercell configuration, there are 84 W atoms and 12 Au atoms in the supercell. The Au atoms adsorbed on the hollow sites of the W(001) surface as shown in Fig. 7(b). Table I shows the interatomic distances between the nearest-neighbor atoms of Au atoms. For the Au atoms at the edge of the Au stripes, there are three nearest-neighbor Au atoms and four nearest-neighbor W atoms. For the case of the other Au atoms, there are four nearest-neighbor Au atoms and four nearest-neighbor W atoms. The interatomic distance between the Au atom and the W atom is less than 2.9 Å; therefore, there is strong chemical bonding between the Au atoms and the W surface atoms.

[1] P. W. Milonni, *The Quantum Vacuum: An Introduction to Quantum Electrodynamics* (Academic Press, San Diego, 1993).

[2] H. B. G. Casimir, Proc. K. Ned. Akad. Wet. **51**, 793 (1948).

[3] A. W. Rodriguez, F. Capasso, and S. G. Johnson, Nat. Photonics **5**, 211 (2011).

[4] J. N. Munday, F. Capasso, and V. A. Parsegian, Nature **457**, 170 (2009).

[5] A. W. Rodriguez, A. P. McCauley, D. Woolf, F. Capasso, J. D. Joannopoulos, and S. G. Johnson, Phys. Rev. Lett. **104**, 160402 (2010).

[6] Y. Luo, R. Zhao, and J. B. Pendry, Proc. Natl. Acad. Sci. USA **111**, 18422 (2014).

[7] A. W. Rodriguez, J. D. Joannopoulos, and S. G. Johnson, Phys. Rev. A **77**, 062107 (2008).

[8] M. Levin, A. P. McCauley, A. W. Rodriguez, M. T. Homer Reid, and S. G. Johnson, Phys. Rev. Lett. **105**, 090403 (2010).

[9] W. J. Kim, A. O. Sushkov, D. A. R. Dalvit, and S. K. Lamoreaux, Phys. Rev. A **81**, 022505 (2010).

[10] R. Zhao, J. Zhou, Th. Koschny, E. N. Economou, and C. M. Soukoulis, Phys. Rev. Lett. **103**, 103602 (2009).

[11] I. G. Pirozhenko and A. Lambrecht, J. Phys. A: Math. Theor. **41**, 164015 (2008).

[12] J. Zou, Z. Marcet, A. W. Rodriguez, M. T. H. Reid, A. P. McCauley, I. I. Kravchenko, T. Lu, Y. Bao, S. G. Johnson, and H. B. Chan, Nat. Commun. **4**, 1845 (2013).

[13] L. Tang, M. Wang, C. Y. Ng, M. Nikolic, C. T. Chan, A. W. Rodriguez, and H. B. Chan, Nat. Photonics **11**, 97 (2017).

[14] L. M. Woods, D. A. R. Dalvit, A. Tkatchenko, P. Rodriguez-Lopez, A. W. Rodriguez, and R. Podgornik, Rev. Mod. Phys. **88**, 045003 (2016).

[15] G. L. Klimchitskaya, U. Mohideen, and V. M. Mostepanenko, Rev. Mod. Phys. **81**, 1827 (2016).

[16] K. Ding, H. Hu, T. C. Leung, and C. T. Chan, ACS Nano **12**, 804 (2018).

[17] G. Kresse and D. Joubert, Phys. Rev. B **59**, 1758 (1999).

[18] G. Kresse and J. Hafner, Phys. Rev. B **47**, 558(R) (1993).

[19] G. Kresse and J. Furthmuller, Comput. Mater. Sci. **6**, 15 (1996).

[20] G. Kresse and J. Furthmuller, Phys. Rev. B **54**, 11169 (1996).

[21] J. P. Perdew, K. Burke, and M. Ernzerhof, Phys. Rev. Lett. **77**, 3865 (1996).

[22] T. C. Leung, C. L. Kao, W. S. Su, Y. J. Feng, and C. T. Chan, Phys. Rev. B **68**, 195408 (2003).